6 Conclusion

The transition metal oxides due to their extraordinary structural and physical properties arising from the coupling of spin, lattice, charge and orbital degree of freedom and various applications like catalytic activity, optoelectronic devices, non-volatile memory, etc., draw considerable attention from thecondensed matter physicists and material scientists. The mixed valence manganese perovskites possess the remarkable phenomena of magnetoresistance which is the unique identity of hole doped manganites. Extensive studies probing the properties of mixed valent manganites $Ln_{1-x}A_xMnO_3$ (A=Ca, Sr, Ba) with perovskite structure have been carried out for almost six decades. The colossal magnetoresistance (CMR) has been a source of great interest for these manganites in recent past due to their potential applications in spintronics, magnetic storage system, magnetic field sensors, solid state, refrigerators and infrared devices. In addition, the perovskites offer diverse physical properties depending on the doping concentration 'x' and preparation route.

In the present work, we have studied the structural, morphological, electronic, magnetic and vibrational properties of$La_{0.67}Sr_{0.33}Mn_{1-x}Fe_xO_3$ (x=0.15, 0.25 and 0.35) compounds synthesized using ball mill (BM) and sol-gel (SG) methods. The properties of these samples are also calculated using *ab–initio* spin-polarized density functional theory and the results are analyzed to understand the formation process of Fe doped LSMO (LSMFO) at different doping concentrations and calcination temperatures. The density functional theory calculations are performed for samples with the help of their own input structural data obtained using x-ray diffraction.

The basic characterization techniques such as XRD, EDAX, FE-SEM, TEM and VSM are used to study the phase purity, elemental details, morphological details, particles size and

magnetic properties of the prepared samples respectively. We have utilized Raman spectroscopy for studying the vibrational properties of LSMFO samples.

The analysis of X-ray diffraction pattern for structural details indicatesthat the compounds are crystallized in rhombohedral, R-3c phase of the space group D^6_{3d} and belongs to the family of rotationally distorted perovskites. The lattice parameters show the Fe content and calcination temperature dependency. There is an increase in lattice parameters and unit cell volume of LSMO samples. The XRD peaks of all the prepared samples by sol-gel route are slightly shifted towards the higher side compared to the ball mill method. The main prominent peak (110) for all the samples that is aligned at 32.7^o for BM route shifts slightly to the lower value in the SG method. This shifting of peak towards lower side reveals that strain is induced due to the dopant ions, also indicating the increase in the degree of long range order in the perovskite host lattice. The shifting towards the lower 2θ, with Fe doping in both synthesis processes indicates the increase in unit cell volume due to close ion radius of Fe and Mn ions at B-site and reduction in internal pressure. The enhancement of volume can be attributed to the enhancement of cell parameters. For a better understanding of the effect of synthesis methods on structural properties, we present the variation of lattice parameters and volume of the unit cell with concentration and calcinations temperature for some selected values in Fig 6.1, which clearly depicts that the trend of variation in lattice parameters and cell volume is more or less similar in both methods. For a fixed calcination temperature, a dip in the value of lattice parameter **c** is observed. The DFT calculated lattice parameters and cell volume obtained for these concentrations corroborate the experimental observations. The effect of increasing Fe content on morphological properties is studied using field emission scanning electron microscopy which shows that the particles are agglomerated. The SEM clearly depicts that the SG method produces particles with smaller size.

The presence of all the corresponding elements in respective prepared samples is confirmed by EDAX and no impurity peak is detected in samples prepared using either method.

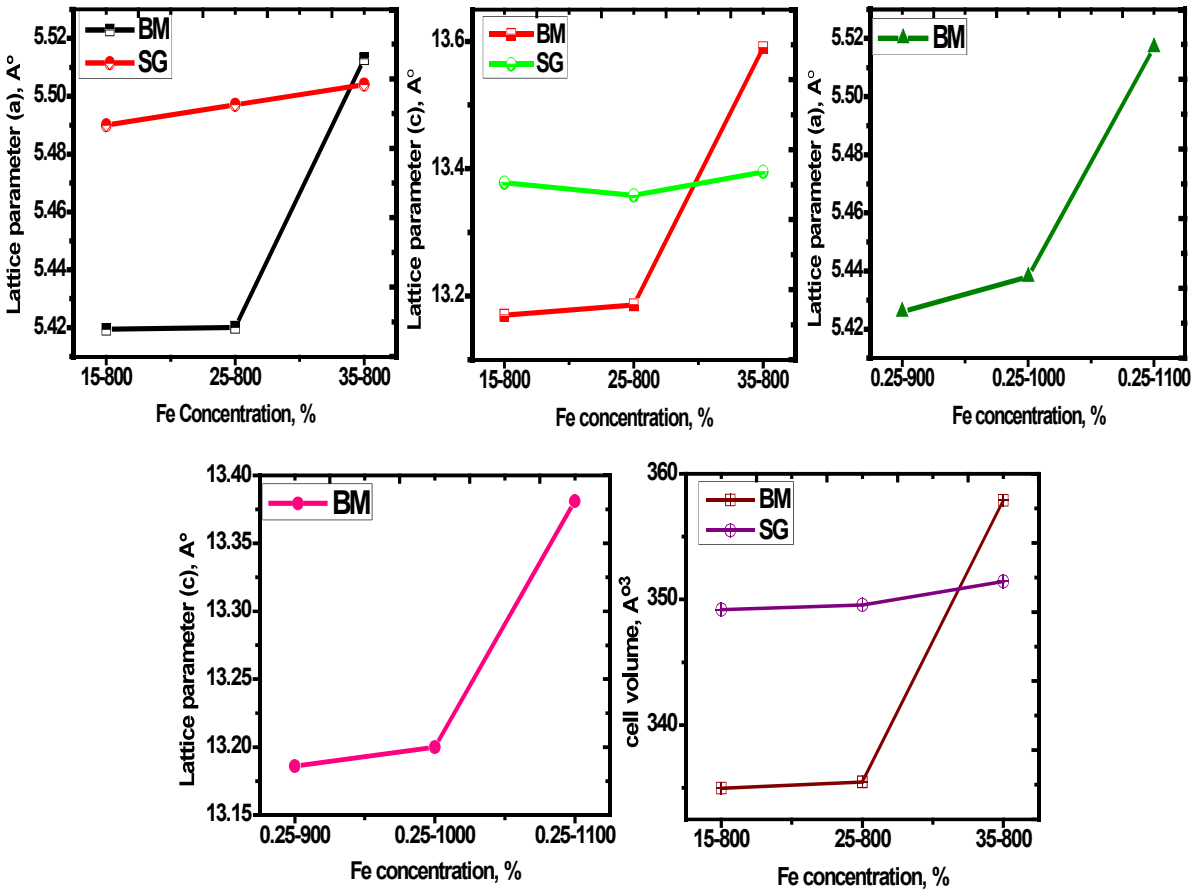

Fig. 6.1: Lattice parameters and unit cell volume of the different concentration of Fe doped LSMO samples.

To understand the electronic and magnetic properties of Fe doped LSMO for various Fe concentrations and calcinations temperatures, spin-polarized density functional theory calculations are performed. This is important not only to have a detailed understanding about electronic and magnetic properties across the several doping concentrations and calcination temperatures but also useful for the systems where experimental study cannot be performed. The spin-polarized calculations performed using local spin density approximation (LSDA) reveal the

metallic behavior without any intimation of antiferrromagnetism for these systems. The Curie temperature (T_C) and magnetic phase transition of selected samples have been investigated using vibrating sample magnetometer. Below Curie temperature, the materials behave like metals and at low temperature, the metal-insulator transition is observed in line with DFT calculations. The saturation magnetization, blocking temperature, magnetic irreversible temperature and Curie temperature increase with increasing doping concentration. The magnetic moment with concentration and temperature increases and decrease respectively. The synthesized LSMFO with nanosize particles show superparamagnetic nature.

The study of vibrational properties of all Fe doped LSMO samples prepared using BM and SG methods is done using Raman spectroscopy, which show significant change in vibrational spectra subjected to Fe ion doping and calcination temperature. Initially, we discuss some of the common features of Raman spectra which give an idea about the JT distortion an important aspect of CMR materials. The nature and shift of peaks reflect the increase/decrease of JT distortion as the peaks directly depend on the motion of the ions in MnO_6 octahedral geometry. The Raman spectra exhibit A_{1g} and E_g modes in rhombohedral Fe doped LSMO. The A_{1g} and E_g modes present in the spectra are due to the motion of oxygen ions at the C_2 sites and La (Sr) site vibrations. The experimental and DFT calculated Raman active A_{1g} and E_g modes are obtained in the range between 221-229 cm^{-1} and 280-308 cm^{-1}, 405-415 cm^{-1} and 670-700 cm^{-1} respectively. The broadening of the peaks indicates an increase in the Jahn-Teller distortion and compression. Also, there is a shift in the peak positions due to increase in the doping concentration, which indicates a change in the MnO_6 octahedral geometry.

Table 6.1 shows the frequency of Raman modes obtained experimentally for the samples of both BM and SG methods together with the DFT calculated Raman modes. We do not present all

data here as it isalready presented in the respective chapters. Further, for SG case, calculations are not performed for all samples due to high computational cost. The A_{1g} peak which arises due to vibrations of oxygen ions at the C_2 sites shows clear shifts toward higher wave number in the case of SG samples then the BM samples. The variation in the BM samples is not consistent. The broad peak in the range between 670-700 cm^{-1} arising due to scattering induced by orthorhombic distortions, shifts towards the higher wave number side in the case of SG samples due to increase in the cell volume and Mn-O distance. A_{1g} and E_g modes which are characteristic modes of manganites arising from the Jahn-Teller distortions clearly show the shifts. While E_g modes near 300 cm^{-1} and 700 cm^{-1} shift toward lower wave number, the $E_g$mode near 400 cm^{-1} shift towards higher wave number particularly in SG method consistent with the DFT calculation. A significant increase in the frequency of the highest E_g mode in the case of SG samples can be attributed to the decrease in Mn-O-Mn bond length, tilting of MnO_6 octahedra and possible insulating high temperature phases. There is a reduction of intensity and increase in broadening of the phonon bands with increase in Fe doping concentration. This indicates that the Fe concentration changes the bond angle and bond length of Mn-O-Mn causing the distortion of octahedron of MnO_6. The E_g and A_{1g} modes, which soften with the concentration, show hardening with the decrease in calcination temperature.

As discussed in chapter 1, the major aim of the present study wasto find which method of sample preparation adopted in the study is more suitable for LSMFO. Apart from studying the electronic and vibrational properties using both experimental and theoretical (density functional theory) methods, it was important to find the process of formation of these samples under different conditions and conclude the suitable conditions for the formation of Fe doped LSMO. For this reason, we calculated the formation energy of the selected samples using DFT.

We limited the computation of formation energy to selected samples to reduce the computational cost as the unit cells of Fe doped LSMO samples are quite large and contains large number of atoms. The formation energy of the samples prepared by BM and SG methods obtained by density functional theory calculations is presented in Table 6.2. The formation energy of Fe doped LSMO manganite sample is minimum for x=0.15 Fe concentration showing the easy formation (thermodynamic stability) of LSMFO samples using both synthesis methods. However, it is expected as seen for the BM method that the higher calcination temperature can result in better formation of Fe doped LSMO.

Table 6.1 Raman frequency of Fe doped LSMO samples at 300 K. The bracket values are DFT data.

Sample	A_{1g}		E_g		E_g		E_g	
	BM	SG	BM	SG	BM	SG	BM	SG
0.15 (800ºC)	224	209	292	296	410	405	670	699
	(226)	(210)	(298)	(301)	(409)	(413)	(686)	(628)
0.25 (800ºC)	225	221	293	281	408	409	675	700
	(229)	(214)	(295)	(294)	(417)	(410)	(671)	(614)
0.35 (800ºC)	221	221	286	290	409	428	675	693
	(223)	(219)	(299)	(264)	(410)	(436)	(661)	(510)

Table 6.2 The calculated formation energy ΔH_F (eV) of Fe doped $La_{0.67}Sr_{0.33}MnO_3$.

Sample	Formation Energy (eV) (BM)	Formation Energy (eV) (SG)
x=0.15 (800ºC)	-5.454	-5.12
x=0.25 (800ºC)	-3.900	-3.56
x=0.35 (800ºC)	-2.110	-1.14
x=0.15 (900ºC)	-5.540	---
x=0.15 (1000ºC)	-5.543	---
x=0.15 (1100ºC)	-5.550	---

The specific conclusions based on the present study are listed below:

1) The Fe doped LSMO samples are prepared using two methods ball milling and sol-gel by varying Fe concentration and calcination temperature.
2) Samples are characterized using XRD, FE-SEM, EDAX, VSM and Raman spectroscopy.
3) The spin-polarized density functional theory is performed to corroborate the experimental findings and to understand the formation of these samples at atomistic level.
4) The XRD pattern shows that the LSMFO samples synthesized using ball-milling and sol-gel methods exhibit the rhombohedral (R-3c) structure.
5) The Fe concentration modifies the frequencies of A_{1g} and E_g Raman modes. However, the changes are more significant in the case of sol-gel prepared samples.

6) The reduction in the intensity of the peaks and increase in broadening with increase in Fe concentration and calcination temperature is observed which arises from the change in bond angle and bond length of Mn-O-Mn causing the MnO_6 octahedron distortion.
7) E_g and A_{1g} modes which soften with the concentration hardens with calcination temperature.
8) The spin-polarized calculations show metallic behavior without any intimation of antiferromagnetism for these systems.
9) The formation energy calculations indicate that the combination of lower concentration of Fe and higher calcination temperature may be suitable condition for the formation of Fe doped LSMO samples. Based on formation energy, the ball mill method shows better thermodynamic stability of the samples. This may be due to the fact that ball milling method involves atomic level mixing while forming a solid compound in which metals of the final product are present in proper stoichiometry.